

A. Kirschner, V. Philipps, M. Balden, X. Bonnin, S. Brezinsek, J.P. Coad, D. Coster, S.K. Erents, H.G. Esser, W. Fundamenski, A. Huber, J. Likonen, H. Maier, G.F. Matthews, M. Mayer, R.A. Pitts, M. Rödiger, M.J. Rubel, U. Samm, J.D. Strachan, M. Wischmeier and JET EFDA contributors

# Material Erosion and Redeposition During the JET MkIIIGB-SRP Divertor Campaign

“This document is intended for publication in the open literature. It is made available on the understanding that it may not be further circulated and extracts or references may not be published prior to publication of the original when applicable, or without the consent of the Publications Officer, EFDA, Culham Science Centre, Abingdon, Oxon, OX14 3DB, UK.”

“Enquiries about Copyright and reproduction should be addressed to the Publications Officer, EFDA, Culham Science Centre, Abingdon, Oxon, OX14 3DB, UK.”

# Material Erosion and Redeposition During the JET MkIIIGB-SRP Divertor Campaign

A. Kirschner<sup>1</sup>, V. Philipps<sup>1</sup>, M. Balden<sup>2</sup>, X. Bonnin<sup>3</sup>, S. Brezinsek<sup>1</sup>, J.P. Coad<sup>4</sup>,  
D. Coster<sup>2</sup>, S.K. Erents<sup>4</sup>, H.G. Esser<sup>1</sup>, W. Fundamenski<sup>4</sup>, A. Huber<sup>1</sup>, J. Likonen<sup>5</sup>,  
H. Maier<sup>2</sup>, G.F. Matthews<sup>4</sup>, M. Mayer<sup>2</sup>, R.A. Pitts<sup>6</sup>, M. Rödiger<sup>7</sup>, M.J. Rubel<sup>8</sup>,  
U. Samm<sup>1</sup>, J.D. Strachan<sup>9</sup>, M. Wischmeier<sup>2</sup> and JET EFDA contributors\*

<sup>1</sup>*Institut für Plasmaphysik, Forschungszentrum Jülich GmbH, EURATOM Association,  
Trilateral Euregio Cluster, 52425 Jülich, Germany*

<sup>2</sup>*Max-Planck-Institut für Plasmaphysik, EURATOM Association, 85748 Garching, Germany*

<sup>3</sup>*CNRS-LIMHP, UPR 1311, Université Paris XIII, F-93430 Villetaneuse, France*

<sup>4</sup>*EURATOM/UKAEA Fusion Association, Culham Science Centre, Abingdon, Oxon OX14 3DB, UK*

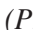
<sup>5</sup>*Association Euratom-Tekes, VTT, Espoo, Finland*

<sup>6</sup>*Centre de Recherches en Physique des Plasmas, Association EURATOM–Confédération,  
Suisse, École Polytechnique Fédérale de Lausanne, CH-1015, Switzerland*

<sup>7</sup>*Heisses Materialprüflabor, B-NM, Forschungszentrum Jülich GmbH, 52425 Jülich, Germany*

<sup>8</sup>*Alfvén Laboratory, Royal Institute of Technology, Association EURATOM–VR, 100 44 Stockholm, Sweden*

<sup>9</sup>*PPPL, Princeton University, Princeton, NJ 08543, USA*

\* See annex of M. L. Watkins et al, "Overview of JET Results",  
(Proc.  IAEA Fusion Energy Conference, Chengdu, China (2006)).

Preprint of Paper to be submitted for publication in Proceedings of the  
21st IAEA Fusion Energy Conference,  
(Chengdu, China, 16th October - 22nd October 2006)



## ABSTRACT.

This contribution provides an overview of experimental results obtained in the area of material erosion and migration during the JET operational campaigns 2002–2004 (C5–C14) with the MkiIGB-SRP divertor configuration and summarises recent modelling activities aimed at understanding these data. Post-mortem analysis of a poloidal tungsten stripe deposited prior the campaigns in the divertor reveals in agreement with previous results that the inner divertor is deposition dominated with maximum layer thicknesses up to 300 $\mu\text{m}$  whereas the outer divertor is erosion dominated in the average over the campaigns. Detailed SEM analysis shows that the outer divertor erosion occurs non-uniformly on a scale length of 10–30 $\mu\text{m}$ . Shot-resolved deposition/erosion measurements with a Quartz MicroBalance (QMB) mounted in the inner divertor louver region demonstrate that the inner strike point position is the most important parameter for the deposition on the QMB with increasing deposition moving the strike point down the vertical target and largest deposition when the strike point is located on the base plate. Data with the strike point on the base plate show a significantly larger deposition in H-mode than in L-mode discharges (about a factor of 20) while this difference is not clearly pronounced with the strike point on the vertical target.  $^{13}\text{CH}_4$  injection through the outer divertor during identical H-mode discharges showed about 75% of the measured  $^{13}\text{C}$  deposition on the outer divertor tiles but also a significant transport of  $^{13}\text{C}$  to the inner divertor and the main chamber region.

## 1. INTRODUCTION

Erosion, material migration and associated problems of long term tritium retention in deposited layers and wall lifetime are among the most critical issues to be solved for ITER [1] and future steady state burning devices. Studying these processes constitutes one of the main research avenues at JET, which is a device dominated presently by carbon walls but also unique both in its use of beryllium (Be) and for its tritium (T) capability. Be-coating by evaporation is done regularly at JET resulting in an average Be content in the plasma of about 8% of the carbon (C) impurity [2]. Tritium is used in dedicated campaigns (e.g. DTE-1 in 1997) including subsequent operation aiming also to explore methods for T recovery. JET is currently preparing an ambitious upgrade, when all C components on the main walls will be replaced with bulk Be tiles or Be-coated Inconel and a full tungsten (W) divertor will be installed. The work on installing the new wall is planned for 2008. Faced with the prospect of a metal wall, consolidation and improvement of our understanding of erosion, deposition and retention under the present all-carbon conditions becomes a high priority task.

This contribution discusses only the main results in the area of material erosion, transport and deposition obtained during the JET MkiIGB-SRP experimental campaigns C5–C14 (2002–2004). Figure 1 shows a cross-section of the MkiIGB-SRP divertor geometry. About 8500 discharges have been executed during these campaigns, which corresponds to a total plasma duration in the divertor phase of about 83000 seconds. Besides different plasma conditions (e.g. L-mode and H-mode) also different plasma configurations, i.e. strike point positions, have been used. The base temperature of

the JET main wall was at 200°C most of the time. The divertor base structure is water-cooled and the C divertor tiles reached a typical baseline temperature of 80 to 140°C.

## **2. CAMPAIGN-INTEGRATED EROSION/DEPOSITION MEASUREMENT BY MEANS OF A TUNGSTEN STRIPE**

Prior to the start of campaign C5 a W-stripe of about 3µm thickness and 2 cm width has been deposited on one poloidal set of divertor tiles at a single toroidal location. Post-mortem analysis of the W-stripe by various surface methods and metallography gave important information on the campaign averaged erosion/deposition behaviour in the divertor.

### ***INNER DIVERTOR:***

Metallographic cross-sections taken from the inner divertor region reveal again that the inner divertor is deposition dominated as shown in figure 2 for the upper vertical tile 1 and for the base tile 4 at two different locations. The W-layer survived in all cases and is covered with a deposit of previous campaigns ( $6.6^{\circ} - 10^{20}$  atoms/s in MkIIA and  $3.5^{\circ} - 10^{20}$  atoms/s in MkIIGB divertor [3]). It should be mentioned that the above-estimated deposition rate for the MkIIGB-SRP campaigns omits a significant amount of the inventory: it does not include deposits on the main wall, on the outer divertor (see next section), on the (shadowed) louver regions and on the Septum Replacement Plate (SRP) and is thus just a lower limit of the overall deposition. Previous measurements revealed that the deposits on the vertical tiles have a typical bulk Be/C ratio of 1:1 whereas the deposits on the shadowed areas of the base plate are carbon rich [2]. Also, ion beam analysis of the vertical tiles 1 and 3 removed in 2004 show similarly large bulk contents of Be in the deposited films [4]. But further analysis is necessary to determine more quantitatively the layer composition.

### ***OUTER DIVERTOR:***

Post-mortem analysis of outer divertor W-coated tiles has been carried out using various surface analysis methods [5] and metallographic cross-sections. In contrast to the inner divertor heavy erosion is observed at the outer vertical tiles with largest erosion at the most heavily loaded tile 7. Figure 3 shows the W areal density before and after operation as measured by Particle Induced X-Ray Emission (PIXE) and Rutherford Backscattering Spectroscopy (RBS). The position of largest erosion on tile 7 corresponds to the maximum in the profile of the deuterium fluence. The vertical tile 8 shows a small erosion consistent with the comparably small fluence to this region (the maximum here is about a factor of 20 smaller than the maximum on tile 7). Surprisingly, the apron of this tile again is heavily eroded although the plasma equilibrium and spectroscopy does not show a significant plasma particle flux there. The reason for the erosion at this area is unclear presently. It is speculated that impurities with higher energies produced by ICRH and LH antennas in the far Scrape-Off-Layer (SOL) may cause this effect.

It would be important to determine the absolute W-erosion rates in particular to draw conclusions concerning the minimum thickness of the W-coatings for the ITER like wall project. The RBS and PIXE analysis suggest that at the heaviest area of erosion still about 30% of the original W-layer

did survive (figure 3), but microscopic analysis reveals (see figure 4, tile 7) that the erosion occurs non-uniformly on scale lengths of 10–30 $\mu\text{m}$ . In certain regions the W-stripe is completely eroded while at neighbouring regions part of the W-layer still exists. Such inhomogeneous erosion has been qualitatively explained by the surface roughness leading to preferential W-erosion of the “hills” which are exposed to larger fluxes and less erosion (or even small deposition) in the “valleys” between the hills.

Modelling of the net-erosion of the W-stripe for tile 7 excluding roughness effects has been done with the Monte-Carlo impurity transport code ERO [6]. Plasma parameters for the simulations are estimated from campaign averaged data with a separatrix temperature of 30eV and density of  $4 \times 10^{18} \text{ m}^{-3}$ . An exponential decay perpendicular to the separatrix is assumed with different decay lengths  $\lambda$  towards the private flux region (PFR,  $\lambda = 4\text{mm}$ ) and the scrape-off layer (SOL,  $\lambda = 12\text{mm}$ ). In toroidal direction symmetry is assumed. A carbon  $\text{C}^{3+}$  background flux of 0.5% relative to the incoming  $\text{D}^+$  flux is assumed and the erosion caused by recycled and redeposited particles is fully included in the modelling. The C-influx of 0.5% is based on the measured averaged total C-wall source from earlier campaigns [7], assuming 50% redeposition of C on the main wall and a transport of the remaining C to the inner and outer divertor with a ratio of 3:1. The modelling shows that the W erosion is dominated by C impurity sputtering whereas the erosion due to deuterium is negligible. About 50% of the sputtered W atoms are redeposited on the W-stripe. Main loss of sputtered W atoms takes place into the PFR originating from a very narrow region around the strike point. With the deuterium fluence distribution along tile 7 taken from calibrated Da photon signals of C5–C14 (taking a S/XB value of 20) and using the ERO results on redeposition and particle recycling, the net erosion profile shown in figure 5 is modelled. The lower limit of the maximum net erosion from the measurement is about 3 $\mu\text{m}$  in fair agreement with the calculated value of about 7 $\mu\text{m}$  at the maximum. Metallographic cross-sections at the outer base plate (tile 6) show deposited layers on the intact W layer, in contrast to the outer vertical tiles. The thickness of the deposits reaches values of up to 200 $\mu\text{m}$ . From this one can estimate an overall deposition of 380g on this tile assuming a density of 1g/cm<sup>3</sup>.

### **3. SHOT-RESOLVED EROSION/DEPOSITION MEASUREMENTS BY MEANS OF A QUARTZ MICROBALANCE**

A Quartz MicroBalance (QMB) has been mounted in 2002 in the inner divertor louver region of MkIIIGB-SRP (see figure 1). It allows a shot-resolved analysis of erosion/deposition at the position of the quartz by monitoring the change of the resonance frequency. A shutter in front of the crystal is used to protect the system from too high power loadings. A second crystal shielded against the particle flux controls the change of the resonance frequency due to changes of the background temperature. The resolution of the QMB is about 1 to 2Hz, which corresponds to one carbon monolayer. More details can be found in [8] and references therein.

The QMB was in operation for a total exposure time (open shutter) of 6479 seconds (806 QMB

exposures). The shot-resolved deposition outside the divertor phase is below the detection limit.

The average deposition rate on the QMB was  $2.8 \times 10^{15}$  C atoms/cm<sup>2</sup>s, which would correspond to a total amount of carbon deposition at the whole inner louver area of about 35g.

This is less than 7% of the overall deposition at plasma-facing components at the inner divertor (about 540g, see section 2). It should be noted that this number is extrapolated from the exposure during about 8% of the whole plasma divertor time. The QMB was normally not exposed for shots with strike points near the inner divertor corner to avoid a QMB overheating. It will be seen that especially this type of shots are expected to produce the largest material deposition at the location of the QMB. However, after the MkIIA campaign about 90% of the carbon deposition in the inner divertor was found at the inner louvers [9] marking a considerable difference to the MkIIIGB and MkIIIGB-SRP campaigns. This difference is attributed to the fact that the strike point during MkIIA was mainly located on the base target. In contrast, during MkIIIGB operation the strike point was mainly on the vertical target and there was a wide variation of strike point positions during MkIIIGB-SRP.

Figure 6 shows the dependence of the QMB signal of the strike point position for 159 discharges in which the position of the strike point has been kept constant (no sweeping). The position in z-direction is related to the plasma configurations used, i.e. strike point at upper part of tile 1 in DOC-U, upper part of tile 3 in DOC-L and lower part of tile 3 in DOC-LL configuration.

In DOC-U discharges the deposition on the QMB is at or below the detection limit of about  $1 \times 10^{15}$  C atoms/cm<sup>2</sup>s. Moving the strike point downwards along the vertical target, the deposition increases up to about  $1 \times 10^{16}$  C atoms/cm<sup>2</sup>s. Largest deposition rates of up to  $\sim 5 \times 10^{16}$  C atoms/cm<sup>2</sup>s are seen if the strike point is located on the base plate with a trend to reach a maximum deposition if the strike point is positioned between the horizontal and inclined part of the base plate. Carbon transport into the louver region is therefore dominated by discharges with the strike point in direct line-of-sight to the louver entrance. This is also consistent with the <sup>13</sup>CH<sub>4</sub> tracer injection from top of the machine in the MkIIIGB divertor configuration with the strike points located on the vertical targets. It has been found, that 99% of the detected <sup>13</sup>C was deposited at the inner vertical divertor tile surfaces [10], see also section 4.

Also ERO code modelling calculations could not produce a significant material deposition on the louvers with plasmas situated on the vertical tiles and show a strong dependence of the deposition at the QMB on strike point position [11]. A reasonable agreement of ERO modelling and average deposition rates in DOC-U, DOC-L and base plate configuration was achieved when erosion by hydrogen atoms has been included and an enhanced (10 times) reerosion of formerly deposited C compared to bulk C material has been assumed. The formation of special layers on the base plate, which are more effectively eroded than graphite is also suggested by spectroscopic observations [12]. If the strike point is moved for the first time to the base plate succeeding discharges with the strike point on the vertical target an enhanced emission of carbon light around the strike point position is observed, in particular enhanced emission from C<sub>2</sub> molecules is large indicating the



presence and erosion of soft carbon layers. By keeping the strike point at the same position on the base plate a successive decrease of carbon light emission occurs. Obviously, discharges with the strike point on the vertical target lead to formation of carbon layers on the base plate, which can be eroded effectively. Thus, the carbon release from the base plate depends on the previous shot history and could be one explanation for the relatively large scatter of the QMB data. On average the deposition in H-mode discharges is larger than in L-mode, again especially in configurations with the strike point on the base plate (see figure 6). Post-mortem analysis revealed coatings on the whole QMB system [13]. On the quartz itself a total amount of about  $9 \times 10^{18}$  C atoms has been detected. The average layer thickness on the quartz is about  $1.85 \mu\text{m}$  which is consistent with the in-situ measured mass increase of about  $1.77 \times 10^{-4}$  g and using a layer density of  $\sim 1 \text{ g/cm}^3$ . Compared to the amount of carbon deposition on the quartz itself, significant deposition of about  $6.2 \times 10^{18}$  atoms has been found at the inner heat shield, visible as colourful layer as shown in figure 7 for the front side of the inner heat shield. This additional contribution has to be taken into account when the overall deposition at the louver region is estimated from the QMB data.

#### 4. $^{13}\text{CH}_4$ TRACER EXPERIMENT AT THE END OF THE EXPERIMENTAL CAMPAIGNS

At the end of the MkiIGB-SRP campaigns  $^{13}\text{C}$  marked methane  $\text{CH}_4$  has been injected into the outer scrape-off layer through a slit between tiles 7 and 8 (figure 1) during 32 consecutive identical type I ELMy H-mode discharges [2]. In total about  $4.3 \times 10^{23}$   $^{13}\text{C}$  atoms have been injected. The magnetic field configuration used for these discharges is indicated in figure 1 with the strike points on the vertical targets. The injected methane flows through 48 toroidally distributed nozzles. No further plasma operation has been done after these discharges before dismounting of tiles and analysing the resulting  $^{13}\text{C}$  deposition distribution. The  $^{13}\text{C}$  deposition averaged over the tiles and integrated toroidally is summarised in table 1. About 20% of the injected  $^{13}\text{C}$  is found on the outer divertor tiles with the highest amount just above the strike point on tile 7. On the inner divertor tiles about 7% of the injected  $^{13}\text{C}$  is detected demonstrating a significant material migration from outer to inner divertor. A significant quantity of  $^{13}\text{C}$  is also transported to the PFR and found on the inner and outer base tiles 4 and 6. First measurements on the shadowed parts of these tiles indicate that the  $^{13}\text{C}$  areal density at these shadowed regions is about a factor of 10 smaller than on the plasma-wetted parts. This confirms, that the transport to such shadowed areas mainly takes place during special shot configurations, i.e. with the strike point on the base target as has been concluded from the QMB data.  $^{13}\text{C}$  also has been found on a fast reciprocating collector probe inserted into each discharge at the top of the low-field side of the poloidal cross-section. This clearly demonstrates that at least part of the material is transported around the main plasma.

EDGE2D modelling has been performed to describe the transport of the injected  $^{13}\text{C}$ . The trajectories of neutrals are calculated with the NIMBUS code and, after ionisation, the fluid model in EDGE2D is applied. The present modelling does not consider the re-erosion of redeposited  $^{13}\text{C}$ . In order to take into account the effect of ELMs, a model describing the increase of transport coefficients

during ELMs has been applied [14]. It is seen that the (longrange) C migration during ELMs is suppressed due to the increased divertor temperature during ELMs, which leads to larger ionisation rates and finally to a larger local redeposition probability. Therefore the long-range C transport mainly takes place during the inter-ELM phases. SOL flows are important for the material transport but the fluid codes still underestimate the high flows measured in the JET SOL. In the EDGE2D modelling the SOL flow is adjusted via an external force to match the measured main chamber SOL flow. The modelling indicates three paths of  $^{13}\text{C}$  migration: most of injected  $^{13}\text{C}$  is deposited on the outer target, a few percent migrates via the main chamber SOL to the inner divertor and a few percent through the PFR into the direction of the inner divertor strike point. Main drawback of the current modelling is considered to be the lack of re-erosion of deposited C. Taking this into account will lead to a change of the transport coefficients used so far in the model such that there may still be agreement between modelled and observed  $^{13}\text{C}$  deposition patterns.

The importance of SOL flows on material migration has also been seen during 4 weeks of plasma operation with reversed magnetic field [15]. It is seen that the asymmetry of plasma parameters between inner and outer divertor is less pronounced compared to operation with usual magnetic field direction (ion grad-B drift points towards the lower X-point). Also, the asymmetric SOL flow from outboard to inboard is strongly reduced during reversed magnetic field operation. Whereas the outer divertor normally is erosion dominated, IR camera observations indicate the formation of layers in the outer divertor during reversed-B [16].

Also at the end of the previous MkiIGB campaign a  $^{13}\text{CH}_4$  injection experiment has been performed, at that time with injection into L-mode discharges from top and the strike points located at the vertical target plates. Experimentally, all  $^{13}\text{C}$  found was inboard from the injection, most of it (99%) on the inner divertor tiles [10] and no  $^{13}\text{C}$  was found in shadowed regions. Modelling (with SOLPS in this case) has shown that a correct description for the carbon sticking and re-erosion must be included to reproduce the  $^{13}\text{C}$  deposition pattern in the inner divertor [17]. Only if the carbon re-enters the plasma after hitting the surface (via reflection or re-erosion) a step-wise material transport to the inner divertor occurs.

## SUMMARY

The JET MkiIGB-SRP campaign has provided new important data in the field of erosion, material migration and deposition. In agreement with all previous results, the post-mortem analysis of a poloidal row of divertor tiles, which have been deposited with a thin W layer in advance, show that the inner divertor is deposition dominated. However, the data show a significant outer divertor net erosion of the W stripe on the vertical tiles, in some contrast to observations from previous campaigns where no clear carbon erosion or deposition was identified. This observation has motivated the use of W coatings of 200 nm thickness within the JET ITER-like wall project. The erosion at the outer vertical divertor could be modelled with the ERO code showing that erosion due to deuterium is negligible compared to the erosion due to carbon impurities.

Shot-resolved measurements of the carbon deposition by means of the QMB show that the carbon transport to this position and other shadowed areas is determined by plasma configurations in which the strike point position offers a direct line-of sight to these areas.

The dependence of the QMB deposition on the strike point position could be reproduced with the ERO code. Spectroscopic observations also indicate that carbon layers, which are built up on the base tiles show an enhanced carbon release when they are first touched by the plasma leading consequently to large material deposition on the QMB. The carbon erosion on specific divertor areas depends therefore on the shot history.

Local injection of methane  $^{13}\text{CH}_4$  into the outer divertor SOL at the end of the experimental campaigns resulted partly in local redeposition near the position of the injection. A significant amount of  $^{13}\text{C}$  is found in the inner divertor that must have been transported through the main plasma or the PFR region. EDGE2D modelling has shown that the longrange carbon transport mainly happens in between ELMs and that three transport paths are required to reproduce the  $^{13}\text{C}$  deposition in the divertor.  $^{13}\text{C}$  has also been found on a deposition probe on top of the machine confirming the C transport way out of the divertor through the main chamber plasma to the inner divertor, but not excluding a possible C transport directly through the PFR in parallel. In the shadowed areas of the divertor little  $^{13}\text{C}$  has been found and, as for the MkIIGB divertor campaign, no beryllium. The overall carbon deposition after the experimental campaign at the divertor, excluding the septum replacement plate, can be estimated to be about 980g corresponding to about  $5.9 \times 10^{20}$  carbon atoms/s, which is similar to previous campaigns. The main deposition of 600g is found in the inner divertor (540g on the inner divertor plates, 60g at the inner divertor louver regions). 380g are deposited at the outer divertor base plate.

## REFERENCES

- [1]. ITER Technical Basis, ITER EDA Documentation Series No 24, IAEA Vienna, 2002
- [2]. J.P. Coad et al., “*Erosion and deposition in the JET MkII-SRP divertor*”, 17th international conference on plasma surface interaction, Hefei, China, 2006
- [3]. V. Philipps, J. Roth, A. Loarte, “*Overview of recent work on carbon erosion, migration and long-term fuel retention in the EU- fusion programme and conclusions for ITER*”, 20th IAEA Conference, Vilamoura, Portugal, 2004
- [4]. J. Likonen et al., “*Structural studies of co-deposited layers on JET MkII-SRP inner divertor tiles*”, 17th international conference on plasma surface interaction, Hefei, China, 2006
- [5]. M. Mayer, “*Tungsten erosion in the outer divertor of JET*”, 17th international conference on plasma surface interaction, Hefei, China, 2006
- [6]. A. Kirschner et al., Nucl. Fus., Vol. **40**, No. 5 (2000) 989
- [7]. J.D. Strachan et al., Nucl. Fus. Vol. **43** (2003) 922
- [8]. H.G. Esser et al., J. Nucl. Mat. **337-339** (2005) 84
- [9]. M.J. Rubel, J. Nucl. Mat. **313-316** (2003) 321

- [10]. J. Likonen et al., Fus. Eng. Des. **66-68** (2003) 219  
 [11]. A. Kirschner et al., J. Nucl. Mat. **337-339** (2005) 17  
 [12]. S. Brezinsek et al., J. Nucl. Mat. **337-339** (2005), 1058  
 [13]. H.G. Esser et al., “*Post mortem analysis of a JET quartz microbalance system*”, 17th international conference on plasma surface interaction, Hefei, China, 2006  
 [14]. A. Kallenbach et al., Plasma. Phys. Contr. Fus. **46** (2004) 431  
 [15]. R.A. Pitts et al., J. Nucl. Mat. **337-339** (2005) 146  
 [16]. P. Andrew et al., J. Nucl. Mat. **337-339** (2005) 99  
 [17]. D.P. Coster et al., “*Integrated modelling of material migration and target power handling at JET*”, 20th IAEA Conference, Vilamoura, Portugal, 2004.

	Tile	$^{13}\text{C}$ amount
Inner	1	2.7%
	3	0.5%
	4	3.8%
Outer	6	2.5%
	7	10.9%
	8	6.1%
<b>Total</b>		<b>26.5%</b>

Table 1: Deposited amount of  $^{13}\text{C}$  measured on divertor tiles (relative to the amount of totally injected  $^{13}\text{C}$ ).

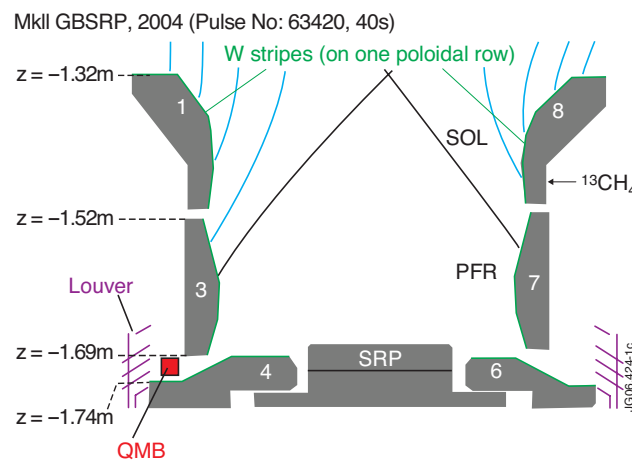


Figure 1: Poloidal cross section of the JET MkIIGB-SRP divertor.

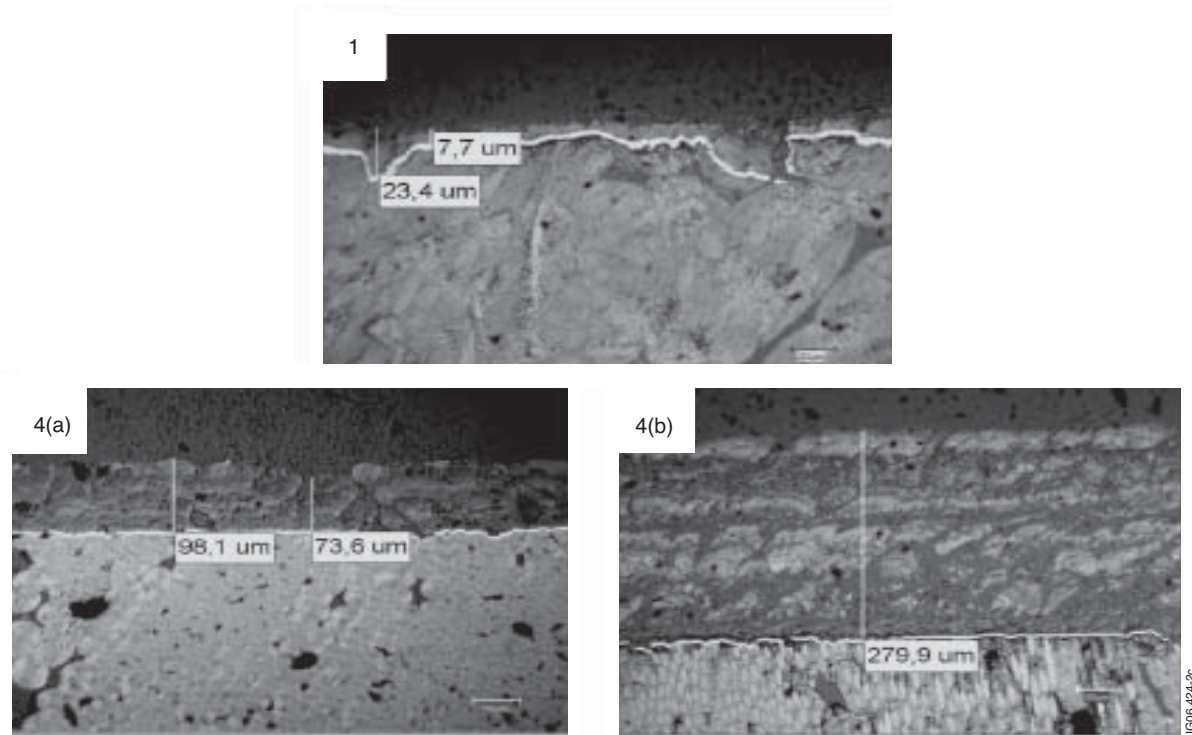


Figure 2: Metallographic cross-sections from samples of inner divertor vertical tile 1 and base tile 4 (4a on horizontal part and 4b on inclined part of tile 4).

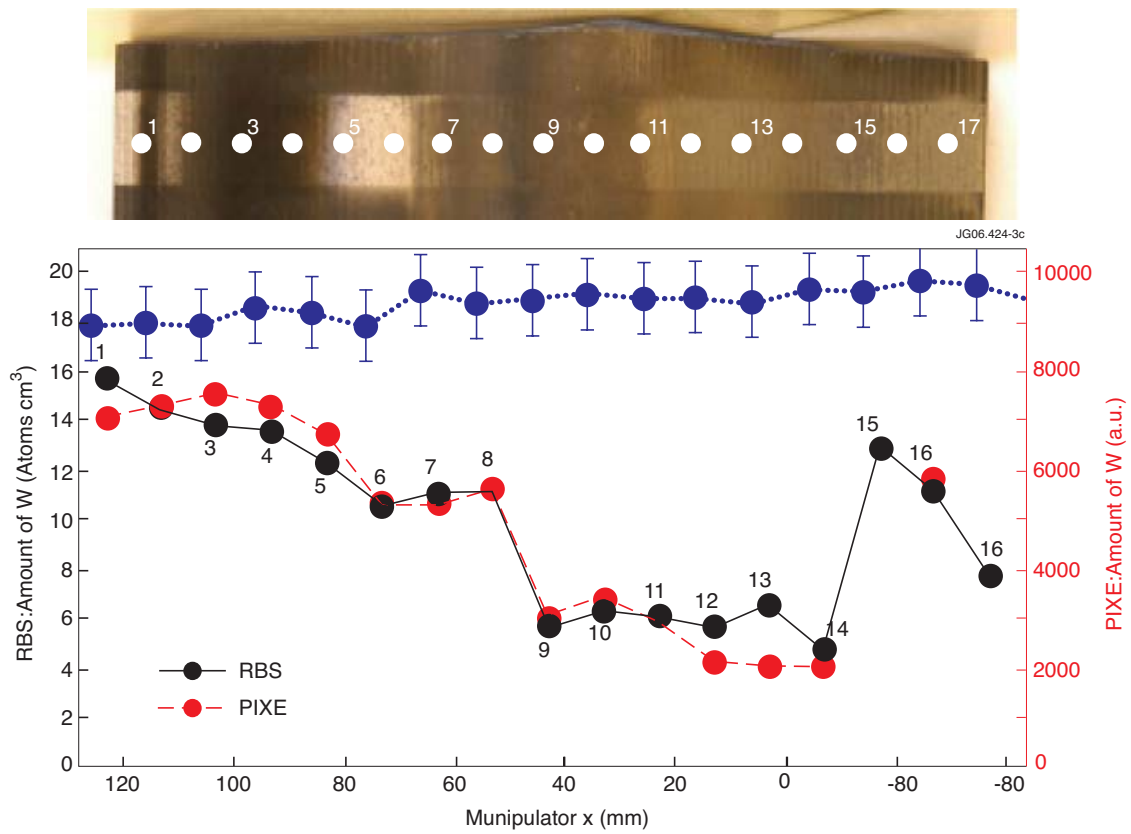


Figure 3: RBS and PIXE profile of the tungsten areal density along outer vertical tile 7.

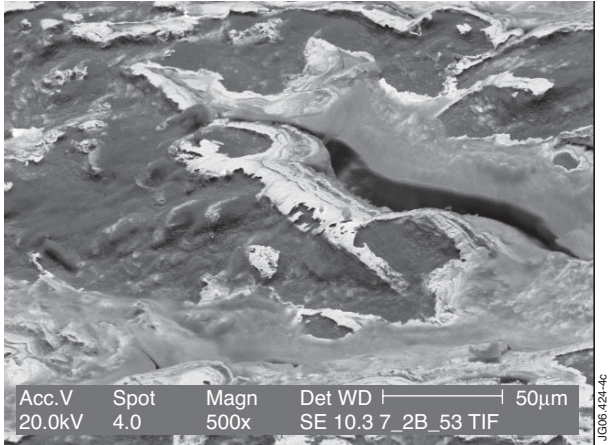


Figure 4: SEM picture from the area of heaviest erosion on outer tile 7.

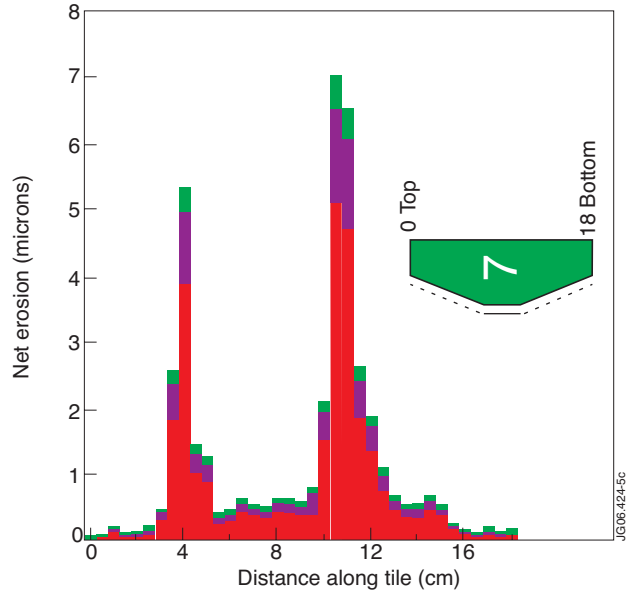


Figure 5: Calculated net tungsten erosion along tile 7 after campaigns C5–C14. Red bars: erosion due to background carbon; Blue bars: erosion due to recycled physically sputtered carbon; green bars: erosion due to recycled chemically eroded carbon.

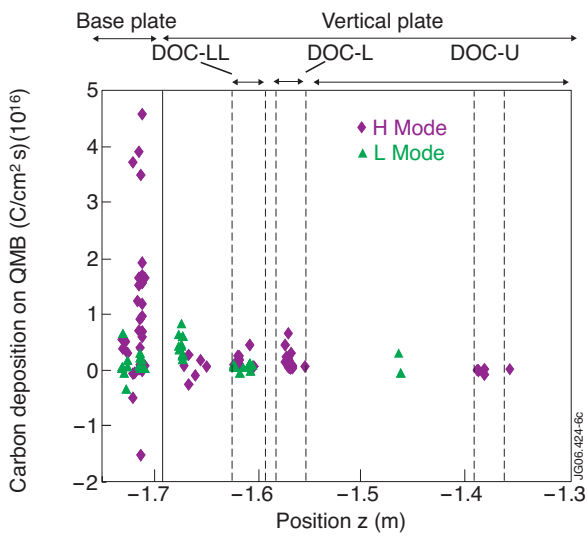


Figure 6: Carbon deposition on the QMB in dependence on strike point position during MkiIGB-SRP campaigns

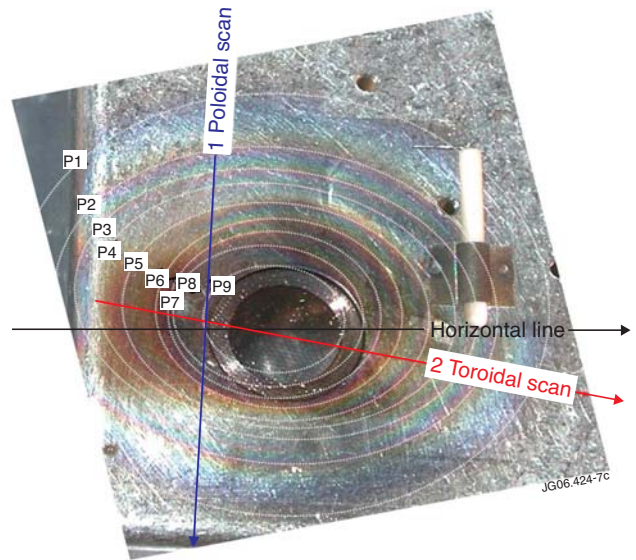


Figure 7: Photograph of front side of the inner heat shield of the QMB.